Loss analysis in nitride deep ultraviolet planar cavity

Zhongming Zheng, Yingqian Li, Baoping Zhang, Hao Long, Samuel Matta, Mathieu Leroux, Julien Brault

Loss analysis in nitride deep ultraviolet planar cavity

Zhongming Zheng[a], Yingqian Li[a], Baoping Zhang[a,*], Hao Long[a], Samuel Matta[b], Mathieu Leroux[b] and Julien Brault[b]

[a] Department of Electronic Engineering, Optoelectronics Engineering Research Center, Xiamen University, Xiamen, Fujian 361005, China

[b] Université Côte d'Azur, CNRS, CRHEA, 06560 Valbonne, France

Abstract. A deep ultraviolet (DUV) nitride planar micro cavity with a double-side HfO_2/SiO_2 DBR structure was fabricated. An AlGaN-based quantum dots (QDs) epilayer was used as the active layer. The epilayers were grown by molecular beam epitaxy (MBE) on sapphire substrate with a thin GaN buffer. Cavity modes at 305, 314, 323 and 335 nm were observed by photoluminescence. Optical losses of the order of 103 cm-1 were deduced from the Q value of the cavity modes. An analysis of the surface scattering losses and absorption of the epilayer was performed. The result suggests that surface scattering from the surface roughness appearing after LLO is the main cause for optical loss,. A method is proposed to reduce the impact of scattering loss by placing the roughness layer at the node of the optical field.

Key words: UV cavity, optical loss, AlGaN-based QDs

*Baoping Zhang, E-mail: bzhang@xmu.edu.cn

1 Introduction

III-nitrides based on $Al_xGa_{1-x}N$ have attracted a lot of attention for promising applications in optoelectronic devices such as ultraviolet laser-diodes (UV-LDs), that have many applications such as high density optical storage, sterilization of water, biological detection and photolithography. $Al_xGa_{1-x}N$ can be used in the ultraviolet regime, with its direct bandgap ranging from 3.4 to 6.0 eV at room temperature by adjusting the Al component[1]. In the last few years, AlGaN-based deep ultraviolet (DUV) edge-emitting lasers have been demonstrated [2-14], with wavelengths ranging from 214 nm[4] to 368.4 nm[5]. The shortest lasing wavelength of electrically injected AlGaN-based laser, at present, is 336 nm[6].

Comparing with edge-emitting lasers, vertical-cavity surface-emitting lasers

(VCSELs) have many advantages such as 1) low power consumption, 2) large scale 2D array, 3) single longitudinal mode operation, 4) circular beam for direct fiber coupling,……[15]. Therefore, the development of UV VCSELs is also very important. VCSELs were firstly proposed by Professor Emeritus Kenichi Iga in 1977[16-18]. The VCSEL lasing action was firstly obtained near 1.2 μm at 77 K in 1979[19]. In recent years, VCSELs have been put to the blue and green range[20-26] using III-nitride semiconductors. However, there were rare reports about VCSELs operating in the UV regime[27-30], and none in the DUV range. And the shortest wavelength optically pumped GaN-based VCSEL reported was operated at 363 nm at 300 K with a threshold of 2 MW/cm^2[29]. All of these epilayers were grown directly on nitride DBRs, and then covered by a dielectric DBR[28, 30] or a nitride DBR[29]. Nitride DBRs are generally characterized by a small refractive index contrast and narrow stop-band width. This will also decrease the confinement factor,due to the large penetration depth of light in nitride DBRs. To get high reflectivity, the period number of DBRs needs to be quite high. It increases the difficulty in material growth. Double-side dielectric DBR structures, by contrast, are preferable. DUV VCSEL operation is also limited by the sub-bandgap absorption in the cavity.

In this work, a DUV double-side dielectric DBR structure planar cavity is reported. Optical losses of the DUV cavity modes were analyzed to be in the 10^3 cm^{-1} range. Theoretical calculations suggest that the scattering loss from the surface, i.e. a roughening of the layer caused by laser lift-off, is the main cause for cavity loss. Fabrication of low-loss DUV resonant cavity is finally discussed.

2 Experimental details

The AlGaN quantum dots (QDs) epilayer was grown on c-plane sapphire by molecular beam epitaxy (MBE) in a RIBER 32 P reactor, following the growth conditions described in ref. [S. Matta, J. Brault, T. H. Ngo, B. Damilano, M. Korytov, P. Vennéguès, M. Nemoz, J. Massies, M. Leroux, and B. Gil, "Influence of the heterostructure design on the optical properties of GaN and $Al_{0.1}Ga_{0.9}N$ quantum dots for ultraviolet emission" J. Appl. Phys. 122, 085706 (2017)]. As shown in Fig. 1, the 30 nm GaN layer was used as a buffer layer and sacrificial layer in the laser lift-off process. Fabrication of the microcavity was then carried out with first coating with a 15 pairs of HfO_2/SiO_2 bottom-DBR, with a peak reflectivity of 98.01% and a bandwidth of ~70 nm, on the top of the sample. It is wider than that of nitride DBR with a peak reflectivity of 98.01% and a bandwidth of 11 nm[30]. After that, the sample was bonded to a quartz glass, faced to bottom-DBR, by wax. And the most important processing technique—laser lift-off (LLO)- was performed with a 248 nm KrF excimer laser to remove the sapphire substrate. Molten Ga was then removed by diluted hydrochloric acid. After that, a 10.5 pairs of HfO_2/SiO_2 top-DBR, with a peak reflectivity of 96.81% and a bandwidth of 69 nm, was deposited on AlN, assuming the whole GaN layer decomposed during LLO. The whole process is schematized in Fig. 2. PL measurements were performed by using the 4th harmonic of a Q-switched Nd: YAG laser with the wavelength of 266 nm as the pumping source. The signal was collected and analyzed by using a spectrometer. The schematic diagram of the PL set-up is depicted in Fig. 3.

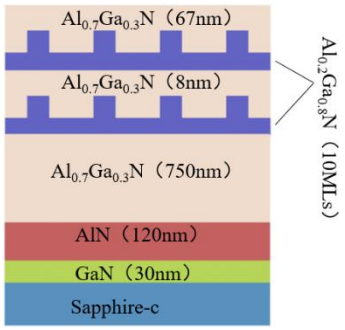

Fig. 1 Schematic diagram of the epilayer

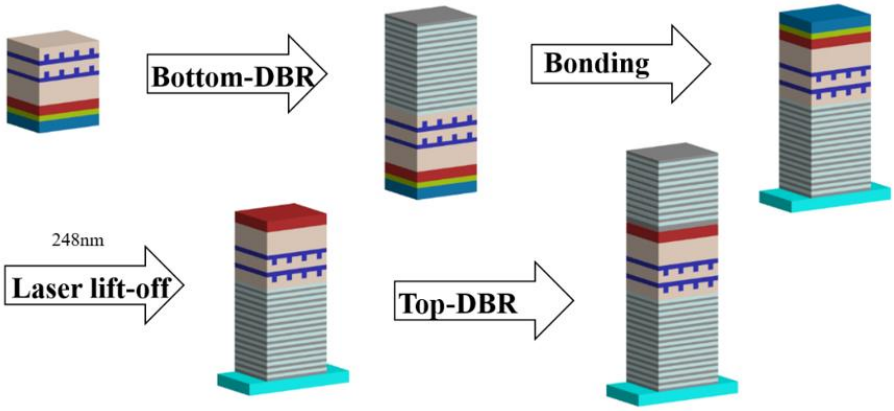

Fig. 2 Diagram of the whole process of fabricating the micro cavity

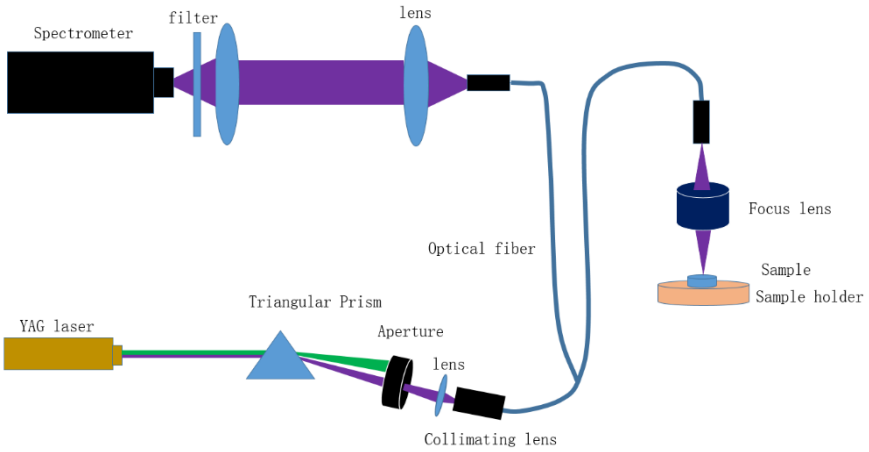

Fig. 3 Schematic diagram of the PL set-up used in this study, a 266 nm wavelength was used as pumping source.

Results and discussion

The PL results are depicted in Fig. 4. One can see that 4 cavity modes are clearly

observed at 305, 314, 323 and 335 nm. Interval among these modes is around 10 nm. The Q value of every mode could be calculated according to equation (1),

$$Q = \lambda_0 / \Delta\lambda , \tag{1}$$

where λ_0 is the peak wavelength of the emission mode, and $\Delta\lambda$ its full width of half maximum. The results are listed in Table 1.

Table 1 Q values and internal cavity losses of every cavity mode

Mode (nm)	305	314	323	335
Q value	166.58	127.32	194.79	160.78
α (cm^{-1})	2671.8	3421.9	2102.5	2363.5

Obviously, the Q values are were low, indicating strong optical losses in the cavity. These optical losses can be deduced from Q according to equation (2),

$$Q = 2\pi \frac{nL_{eff}}{\lambda} \left(\frac{1}{\ln\left(R_{b\_DBR} R_{t\_DBR}\right)^{-1/2} + L_{eff}\alpha} \right), \tag{2}$$

where n is the cavity refractive index, L_{eff} is the effective cavity length, λ is the wavelength, α is the internal cavity loss, R_{t_DBR} and R_{b_DBR} are the top and bottom DBR reflectivities, respectively. The effective cavity length L_{eff} is longer than the nominal thickness of the epilayer，due to the limited controllability, and could be obtained from equation (3),

$$v_{q+1} - v_q = \frac{c}{2nL_{eff}}, \tag{3}$$

where q is the longitudinal mode order, v is the longitudinal mode frequency, c is the vacuum light velocity. L_{eff} was then evaluated to be 2288 nm. And cavity losses of every mode were 2671.8, 3421.9, 2102.5, and 2363.5 cm^{-1} for the 305, 314, 323, and 335 nm modes, respectively (Table 1). If the cavity loss reduces to 195 cm^{-1}，the Q

value will reach 1500.

Fig. 5 depicts the simulated cavity modes distributions and the refractive index profile. Simulated effective cavity lengths (L_{eff}), corresponding to every mode, can also be obtained from these curves between the two positions where the optical intensity decreases to 1/e, and the confinement factors (Γ_r) are then also obtained. The definition of the confinement factor is :

$$\Gamma_{\mathrm{r}} = \frac{L_{eff}}{d_a} \frac{\int_{d_a} |E(z)|^2 \, dz}{\int_{L_{eff}} |E(z)|^2 \, dz}, \tag{4}$$

where d_a is active region thickness, $E(z)$ is the electric field intensity along the z axis. The results are listed in Table 2. A Γ_r value close to 2 suggests that the active region is perfectly aligned to the antinode of the cavity mode.

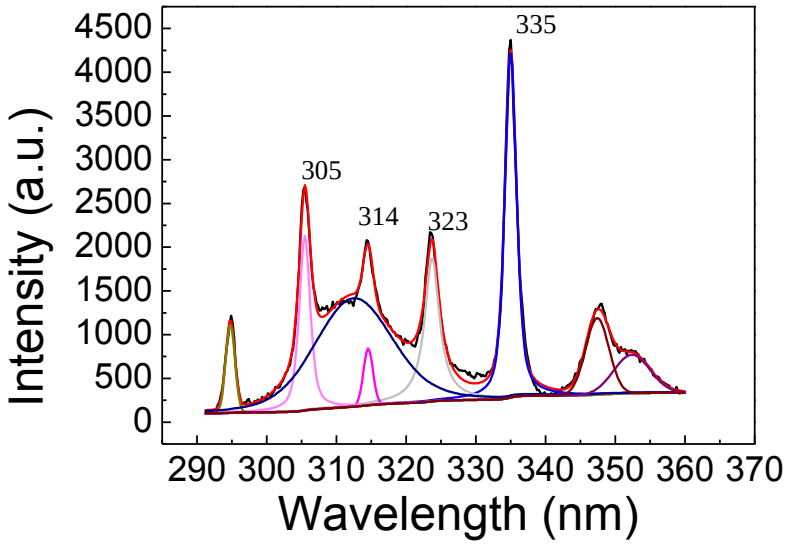

Fig. 4 Emission spectra of the micro cavity at which temperature ?

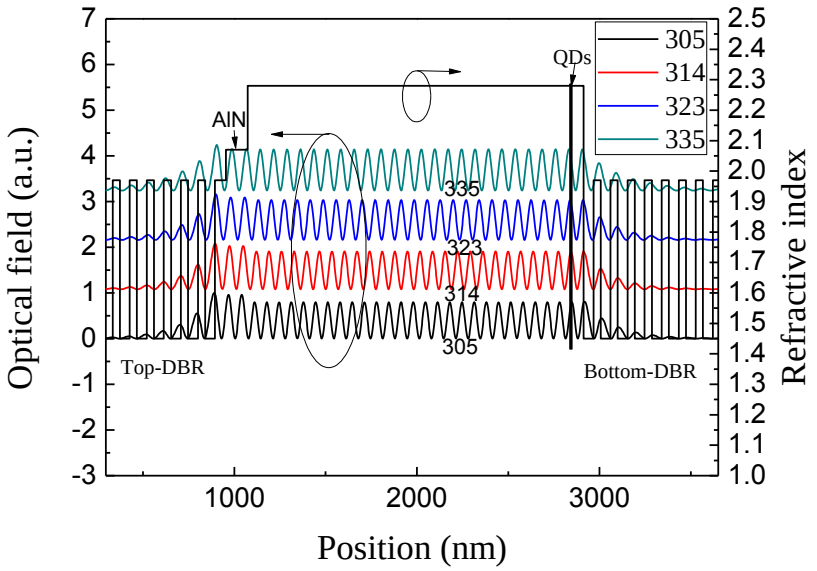

Fig. 5 Simulated cavity modes distributions and refractive index profiles

Table 2 Confinement factor, reflectance of bottom and top DBR and overlap area of the sample

Mode (nm)	305	314	323	335
Γ_r	1.71	1.89	1.88	1.62
R_{b_DBR}(%)	98.01	97.97	97.66	96.74
R_{t_DBR}(%)	96.81	96.64	95.70	91.56
OA	17.13	14.97	11.44	7.14

The surface morphology of the epilayer after LLO had been characterized by atomic force microscopy (AFM), as shown in Fig. 6. Over a 10 μm ×10 μm area, the root mean square (RMS) of the surface roughness was about 20.36 nm. When the surface roughness is far below the incident wavelength, scattering losses can be defined as the total integrated scattering (*TIS*)[31], i.e. the ratio between scattering by surface and total reflection by surface, as in equation (5),

$$TIS = C\left\{1-\exp\left[-\left(\frac{4\pi\delta\cos\theta}{\lambda_0}\right)^2\right]\right\}, \quad (5)$$

where δ is the RMS of the surface roughness, θ is the incident angle, λ_0 is the wavelength, and C is a correction factor, which is equal to 0.96. If light travels from

the opposite direction, C will be 1/0.96=1.04. For normal incidence (θ=0), the *TIS* for the 305, 314, 323 and 335 nm modes are 49%, 47%, 45% and 42%, respectively. It suggests that theses roughness scattering losses dominate in the cavity losses.

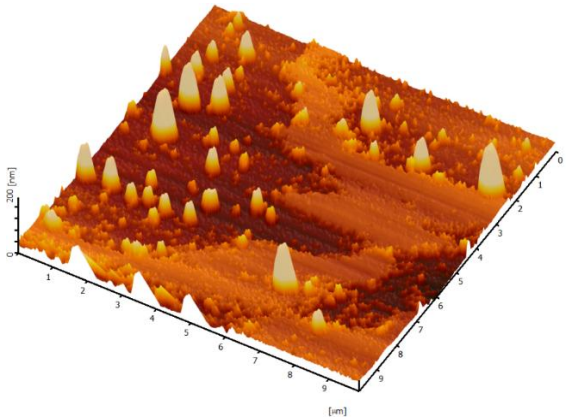

Fig. 6 Surface morphology of the epilayer after LLO characterized by AFM

The absorption of the epilayer, which was mainly composed of $Al_{0.7}Ga_{0.3}N$ with an absorption coefficient about 0.45×10^3 cm^{-1} near 320 nm[32], was also calculated. The absorbance of the epilayer (A_{epi}) could be evaluated according to equation (6),

$$A_{epi} = 1 - e^{-\alpha_{epi} d}, \tag{6}$$

where α_{epi} is the absorption coefficient, and d is the layer thickness. The absorbance of the epilayer (A_{epi}) through the thickness of the epilayer was 8.4%. The average percentage of optical losses (A_{ave}) in a single round trip can be deduced from Fig. 7. When light travels from the assumptive starting point, S, A_{ave} is given as :

$$\begin{aligned} A_{ave} &= 1-(1-A_{epi})(1-TIS)R_{t\_DBR}(1-TIS')(1-A_{epi})R_{b\_DBR} \\ &= 1-(1-A_{epi})^2(1-TIS)(1-TIS')R_{b\_DBR}\,R_{t\_DBR}, \end{aligned} \tag{7}$$

where R_{b_DBR} and R_{t_DBR} are the bottom and top DBR reflectivities, respectively, listed in Table 2. *TIS'* is when light travels in the opposite direction compared with *TIS*. And *TIS'* for 305, 314, 323 and 335 nm modes are 53%, 51%, 49% and 46%,

respectively. The absorbance of the DBR was omitted, since the values of the bottom and top DBR were negligeable, i.e. respectively far below 0.9% and 3.0%, and therefore complicated to observe. The result was

$$A_{ave}=1-(1-8.4\%)^2(1-45.75\%)(1-49.75\%)*97.6\%*95.18\%=78.75\% . \quad (8)$$

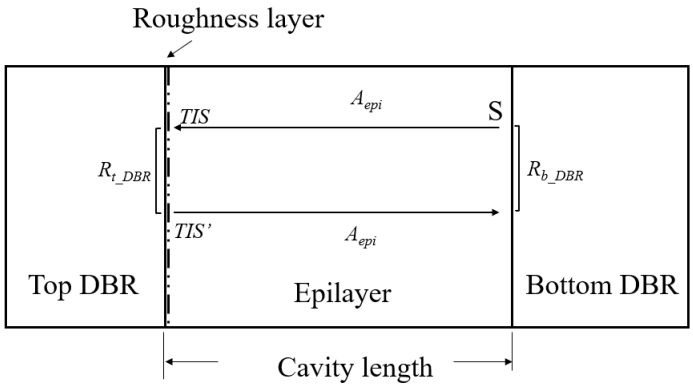

Fig. 7 Schematic diagram of a single round trip of light traveling in the cavity

A_{ave} has a huge value and will largely increase the threshold of lasing. Obviously, the *TIS* is the dominant factor in the optical losses of the cavity. If *TIS* and *TIS'* are omitted, the value of A_{ave} would decrease to 22.06%. If only *TIS* and *TIS'* were taken into account, the value would be equal to 72.74%. The next work should focus on reducing the *TIS*, i.e. on reducing the surface roughness.

To reduce the optical losses at the interface between the top-DBR and the epilayer, one method is proposed in the following. Fig. 8 represents a zoom of Fig. 5, i.e. the simulated cavity modes, with the red rectangle indicating the rough layer generated by LLO. It is shown that if this layer is properly placed at the node of the standing wave, the scattering losses will be minimized. Also, the LLO processing technique should be continuously improved to reduce the surface roughness: for instance, reducing its value to 1 nm should lead to a *TIS* of 0.0015 and the Q value will be increased to

around 700.

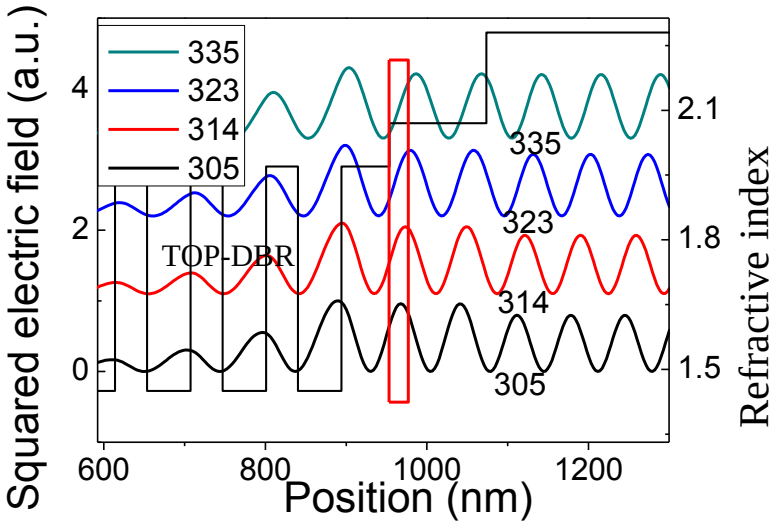

Fig. 8 Investigation of the coupling of the interfacial layer (see Fig. 7) between the top DBR and the epilayer (red rectangle) and the optical field in the laser cavity

At last, we focus on the observed peak intensity differences among these cavity modes. Fig. 4 shows that the optical intensity of the 335 nm mode is the strongest, followed by the 323 nm mode, the third is the 305 nm mode, and the 314 nm mode is the weakest. Calculations of overlap areas (OA) of the optical field of each cavity mode with the (rough) interfacial layer are performed, from Fig. 8 simulations. The results are listed in Table 2. These values can be used to evaluate the influence of the scattering losses on the cavity modes, i.e. the bigger the value is, the greater impact it has. Obviously, the OA of 314 nm, 323 nm and 335 nm modes are decreasing with the wavelength increase, which means that the impact of the scattering losses is larger for the 314 nm mode, in agreement with our results. However, the 305 nm mode presents an abnormal behaviour, since its intensity is higher than that of the 314 nm mode. At this stage, the origin of this characteristic is still unclear. Regarding the

335nm mode of smaller Q value than that of the 323 nm mode, it could be attributed to the lower reflectivities of the DBRs. In addition, according to equation (5), scattering losses also increase with decreasing wavelength and actually the 314 nm, 323 nm and 335 nm modes all followed this rule. In our study, except for the 305 nm mode, OA and scattering losses have been found to increase with decreasing wavelength.

Conclusions

To sum up, an AlGaN-based QDs microcavity with double-sided dielectric DBRs structure was fabricated and optical losses were analyzed. The optical loss was 10^3 cm^{-1} in magnitude and found to be mainly caused by surface roughness scattering after the LLO process. Improvements for reducing the surface scattering losses were proposed by properly placing the epilayer – top DBR interface at a node of the optical field.

Acknowledgements

This work was supported by the National Key R&D Program of China (No.2016YFB0400803), the National Natural Science Foundation of China (Nos. 11474235, U1505253) and the Science Challenge Project (No. TZ2016003). The epilayer used in this work was grown by CNRS-CRHEA. J. B., S. M. and M. L. acknowledge partial support from the ANR Project <ANR-14-CE26-0025-01> “NANOGANUV”.

References

[1] Koide Y, Itoh H, Khan M R H, et al. Energy band‐gap bowing parameter in an AlxGa1−x N alloy[J]. Journal of Applied Physics, 1987, 61(9): 4540-4543.

[2] Iida K, Kawashima T, Miyazaki A, et al. 350.9 nm UV Laser Diode Grown on Low-Dislocation-Density AlGaN[J]. Japanese Journal of Applied Physics, 2004, 43(No. 4A): L499-L500.

[3] Takano T, Narita Y, Horiuchi A, et al. Room-temperature deep-ultraviolet lasing at 241.5 nm of AlGaN multiple-quantum-well laser[J]. Applied Physics Letters, 2004, 84(18): 3567-3569.

[4] Shatalov M, Gaevski M, Adivarahan V, et al. Room-Temperature Stimulated Emission from AlN at 214 nm[J]. Japanese Journal of Applied Physics, 2006, 45(No. 49): L1286-L1288.

[5] Kneissl M, Yang Z, Teepe M, et al. Ultraviolet semiconductor laser diodes on bulk AlN[J]. Journal of Applied Physics, 2007, 101(12): 123103.

[6] Yoshida H, Yamashita Y, Kuwabara M, et al. Demonstration of an ultraviolet 336 nm AlGaN multiple-quantum-well laser diode[J]. Applied Physics Letters, 2008, 93(24): 241106.

[7] Jmerik V N, Mizerov A M, Sitnikova A A, et al. Low-threshold 303 nm lasing in AlGaN-based multiple-quantum well structures with an asymmetric waveguide grown by plasma-assisted molecular beam epitaxy on c-sapphire[J]. Applied Physics Letters, 2010, 96(14): 141112.

[8] Wunderer T, Chua C L, Yang Z, et al. Pseudomorphically Grown Ultraviolet C Photopumped Lasers on Bulk AlN Substrates[J]. Applied Physics Express, 2011, 4(9): 092101.

[9] Jmerik V N, Lutsenko E V, Ivanov S V. Plasma-assisted molecular beam epitaxy of AlGaN heterostructures for deep-ultraviolet optically pumped lasers[J]. Physica Status Solidi, 2013, 210(3): 439-450.

[10] Lochner Z, Kao T-T, Liu Y-S, et al. Deep-ultraviolet lasing at 243 nm from photo-pumped AlGaN/AlN heterostructure on AlN substrate[J]. Applied Physics Letters, 2013, 102(10): 101110.

[11] Ivanov S V, Nechaev D V, Sitnikova A A, et al. Plasma-assisted molecular beam epitaxy of Al(Ga)N layers and quantum well structures for optically pumped mid-UV lasers on c-Al2O3[J]. Semiconductor Science & Technology, 2014, 29(29): 084008.

[12] Li X-H, Detchprohm T, Kao T-T, et al. Low-threshold stimulated emission at 249 nm and 256 nm from AlGaN-based multiple-quantum-well lasers grown on sapphire substrates[J]. Applied Physics Letters, 2014, 105(14): 141106.

[13] Martens M, Mehnke F, Kuhn C, et al. Performance Characteristics of UV-C AlGaN-Based Lasers Grown on Sapphire and Bulk AlN Substrates[J]. IEEE Photonics Technology Letters, 2014, 26(4): 342-345.

[14] Yan J, Tian Y, Chen X, et al. Deep ultraviolet lasing from AlGaN multiple-quantum-well structures[J]. physica status solidi (c), 2016, 13(5-6): 228-231.

[15] Koyama F. Advances and New Functions of VCSEL Photonics[J]. Optical Review, 2014, 21(6): 893-904.

[16] Iga K. Vertical-cavity surface-emitting laser: Its conception and evolution[J]. Japanese Journal Of Applied Physics, 2008, 47(1): 1-10.

[17] Iga K, Ieee. VCSEL -Its Conception, Development, and Future[J]. 2013 18th Microoptics Conference (Moc), 2013: 2.

[18] Iga K, Koyama F, Kinoshita S. SURFACE EMITTING SEMICONDUCTOR-LASERS[J]. Ieee Journal Of Quantum Electronics, 1988, 24(9): 1845-1855.

[19] Soda H, Iga K, Kitahara C, et al. GaInAsP/InP Surface Emitting Injection Lasers[J]. Japanese Journal of Applied Physics, 1979, 18(12): 2329-2330.

[20] Mei Y, Xu R-B, Weng G-E, et al. Tunable InGaN quantum dot microcavity light emitters with 129 nm tuning range from yellow-green to violet[J]. Applied Physics Letters, 2017, 111(12): 121107.

[21] Hamaguchi T, Fuutagawa N, Izumi S, et al. Milliwatt-class GaN-based blue vertical-cavity surface-emitting lasers fabricated by epitaxial lateral overgrowth[J]. Physica Status Solidi a-Applications And Materials Science, 2016, 213(5): 1170-1176.

[22] Izumi S, Fuutagawa N, Hamaguchi T, et al. Room-temperature continuous-wave operation of GaN-based vertical-cavity surface-emitting lasers fabricated using epitaxial lateral overgrowth[J]. Applied Physics Express, 2015, 8(6): 062702.

[23] Omae K, Higuchi Y, Nakagawa K, et al. Improvement in Lasing Characteristics of GaN-based Vertical-Cavity Surface-Emitting Lasers Fabricated Using a GaN Substrate[J]. Applied Physics Express, 2009, 2: 052101.

[24] Lu T-C, Kao C-C, Kuo H-C, et al. CW lasing of current injection blue GaN-based vertical cavity surface emitting laser[J]. Applied Physics Letters, 2008, 92(14): 141102.

[25] Feltin E, Christmann G, Dorsaz J, et al. Blue lasing at room temperature in an optically pumped lattice-matched AlInN/GaN VCSEL structure[J]. Electronics Letters, 2007, 43(17): 924-926.

[26] Mei Y, Weng G-E, Zhang B-P, et al. Quantum dot vertical-cavity surface-emitting lasers covering the ‘green gap’[J]. Light: Science & Applications, 2016, 6(1): e16199-e16199.

[27] Liu Y-S, Kao T-T, Mehta K, et al., 'Development for Ultraviolet Vertical Cavity Surface Emitting Lasers', in *Gallium Nitride Materials And Devices Xi*, ed. by J. I. Chyi, H. Fujioka, H. Morkoc, Y. Nanishi, U. T. Schwarz and J. I. Shim, 2016).

[28] Zhou H, Diagne M, Makarona E, et al. Near ultraviolet optically pumped vertical cavity laser[J]. Electronics Letters, 2000, 36(21): 1777-1779.

[29] Redwing J M, Loeber D A S, Anderson N G, et al. An optically pumped GaN–AlGaN vertical cavity surface emitting laser[J]. Applied Physics Letters, 1996, 69(1): 1-3.

[30] Liu Y-S, Saniul Haq A F M, Mehta K, et al. Optically pumped vertical-cavity surface-emitting laser at 374.9 nm with an electrically conducting n-type distributed Bragg reflector[J]. Applied Physics Express, 2016, 9(11): 111002.

[31] Guenther K H, Wierer P G, Bennett J M. Surface roughness measurements of low-scatter mirrors and roughness standards[J]. Applied Optics, 1984, 23(21): 3820-3836.

[32] Brunner D, Angerer H, Bustarret E, et al. Optical constants of epitaxial AlGaN films and their temperature dependence[J]. Journal Of Applied Physics, 1997, 82(10): 5090-5096.